Symmetry-breaking instability and strongly peaked periodic clustering states in a driven granular gas

Eli Livne,[1] Baruch Meerson,[1] and Pavel V. Sasorov[2]
[1]*Racah Institute of Physics, Hebrew University of Jerusalem, Jerusalem 91904, Israel*
[2]*Institute of Theoretical and Experimental Physics, Moscow 117259, Russia*
(Received 21 August 2000; revised manuscript received 17 July 2001; published 9 January 2002)

An ensemble of inelastically colliding grains driven by a horizontally vibrating wall in two dimensions exhibits clustering. Working in the limit of nearly elastic collisions and employing granular hydrodynamics, we predict, by a marginal stability analysis, a spontaneous symmetry breaking of the laterally uniform clustering state. Two-dimensional steady-state solutions found numerically describe laterally periodic clustering states. Well within the instability region the density of these states is strongly peaked, with most of the granulate located in ''density islands.'' Time-dependent granular hydrodynamic simulations show that strongly peaked states can develop from small-amplitude single-mode density perturbations.

DOI: 10.1103/PhysRevE.65.021302 PACS number(s): 81.05.Rm, 45.70.Qj, 47.50.+d

I. INTRODUCTION

Granular flows exhibit fascinating nonequilibrium phenomena and continue to attract much interest [1,2]. We will concentrate here on the striking tendency of granular ''gases'' (rapid granular flows) to form dense clusters [3]. Clustering results from energy losses by inelastic collisions, and it is a manifestation of thermal condensation instability, also known in other media [4]. Since the discovery of the clustering instability, the validity of granular hydrodynamics [5] has been under scrutiny. In a freely cooling granular gas, all grains eventually come to rest, making a hydrodynamic (and even kinetic) description problematic. In a *driven* granular gas hydrodynamics can be conveniently tested on its steady states. The simplest system of this kind is a submonolayer of grains in two dimensions, driven by a vibrating sidewall at zero gravity. This and related ''test bed'' systems have been investigated by molecular dynamic (MD) simulations [6–8] and in experiment [9]. For sufficiently high average densities a clustering state was observed in these works away from the driving wall. This clustering state was almost uniform in the lateral direction in rectangular boxes [6,7,9], and in the azimuthal direction in a circular box [8]. We will call this laterally (or azimuthally) uniform clustering state an ''extended clustering state'' (ECS). The basic physics of the ECS is simple. Because of the inelastic collisions the granular temperature decreases with increasing distance from the driving wall. To maintain the momentum balance, the granular density should increase with this distance, reaching the maximum at the opposite (''elastic'') wall. When the density contrast is large enough, the enhanced density region is observed as the ECS.

Comparisons of the steady-state density profiles obtained in MD simulations of this class of problems with those predicted by granular hydrodynamics showed that hydrodynamics is valid only in the limit of nearly elastic collisions [6–8,10]. This limit has not been fully explored, and it is nontrivial. To demonstrate it, we start with a marginal stability analysis of this simplest granular system. This analysis reveals a symmetry-breaking instability of the ECS, and formation of laterally periodic clustering states. Then we investigate nonlinear steady states of this system numerically. We find that, well within the instability region, the density of the laterally periodic clustering states is strongly peaked. Finally, we report a series of time-dependent granular hydrodynamic simulations that show that strongly peaked clustering states develop from small-amplitude single-mode density perturbations.

II. MODEL PROBLEM AND LATERALLY UNIFORM CLUSTERING STATE

Consider a big ensemble of identical spherical grains of diameter d and mass $m_g=1$ rolling on a smooth horizontal surface of a rectangular box with dimensions $L_x\times L_y$. The limit of $L_y\to\infty$ corresponds to an infinite strip. This important limit will also be considered. The number density of grains is $n(x,y)$. For a submonolayer coverage the maximum value of n corresponds to the (hexagonal) close-packing value $n_c=2/(\sqrt{3}d^2)$. Three of the walls are immobile, and grain collisions with them are assumed elastic. The fourth wall (located at $x=L_x$) supplies energy to the granulate. We will consider two different models of energy supply (see below). The energy is being lost through inelastic hard-core grain collisions. We neglect the grain rotation and parametrize the inelasticity of grain collisions by a constant normal restitution coefficient r.

We assume a *strong* inequality $1-r^2\ll 1$, which makes a hydrodynamic description valid [6–8]. Therefore, steady states of the system can be described by the equations of momentum and energy balance:

$$p=\text{const}, \quad \nabla\cdot(\kappa\nabla T)=I, \tag{1}$$

where p is the granular pressure, κ is the thermal conductivity, I is the rate of energy losses by collisions, and T is the granular temperature. To proceed, one needs an equation of state $p=p(n,T)$ and relations for κ and I in terms of n and T. In the low-density limit $n\ll n_c$, these relations can be derived from the Boltzmann equation [5]. The high-density limit $n_c-n\ll n_c$ was considered by Grossman *et al.* [6].

They also suggested convenient interpolations between the low- and high-density limits, and verified them by a detailed comparison with MD simulations. We will adopt this practical approach (see, however, Sec. IV). In our notation

$$p = nT\frac{n_c+n}{n_c-n}, \tag{2}$$

$\kappa=(\mu/l)n(\alpha l+d)^2T^{1/2}$, and $I=(\mu/\gamma l)(1-r^2)nT^{3/2}$. Here l is the mean free path of the grains,

$$l=\frac{1}{\sqrt{8}nd}\frac{n_c-n}{n_c-an}, \tag{3}$$

$a=1-(3/8)^{1/2}$, and α and γ are numerical factors of order unity. Grossman *et al.* [6] found that $\alpha\simeq 1.15$ and $\gamma\simeq 2.26$. The value of μ, another numerical factor of order unity, is irrelevant in the steady-state problem.

The boundary conditions include the no-flux conditions $\boldsymbol{\nabla}_n T=\mathbf{0}$ at the ''elastic'' walls $x=0$, $y=0$, and $y=L_y$ ($\boldsymbol{\nabla}_n$ means the component of the gradient normal to the wall). Previously, the ''thermal'' wall condition $T=$const was used at $x=L_x$ [6–8,12]. We will use a different boundary condition, to simulate the vibrating wall more directly. Our main results, however, will be shown to hold for the thermal wall as well. When the system is infinite in the lateral direction, $L_y=\infty$, only two boundary conditions remain, at $x=0$ and $x=L_x$.

The problem of computing the energy flux q from a vibrating wall into granulate has been addressed in several works [13]. Let the wall oscillate sinusoidally: $x=L_x+A\cos\omega t$. For small area fractions the granulate near this wall is in the dilute limit. We assume $A\ll l$, so the vibrating wall does not generate any collective motions in the granulate. Grain collisions with the vibrating wall are assumed elastic. Also, ω is much larger than the rate of granular collisions near the vibrating wall, $T^{1/2}/l$, so there are no correlations between two successive grain collisions with the wall. The limit $A\omega\ll T^{1/2}$ was considered by Kumaran [14] for a nonzero gravity. We will work in this regime. Direct calculations analogous to that of Kumaran [14], but for zero gravity, yield $q=(2/\pi)^{1/2}A^2\omega^2nT^{1/2}$ In the language of hydrodynamics, q is the heat flux at the wall:

$$\kappa\,\partial T/\partial x = q \quad \text{at } x=L_x. \tag{4}$$

For this hydrodynamic relation to be valid, l calculated near the wall should be much smaller than the characteristic length scale of the gas phase, which, for typical parameters we are interested in (see below), is close to $\min(L_x,L_y)$. Finally,

$$\frac{1}{L_xL_y}\int_0^{L_x}\int_0^{L_y} n(x,y)\,dx\,dy=\langle n\rangle=\text{const}$$

is a normalization condition, where $\langle n\rangle$ is the average grain density.

Using Eq. (2), we eliminate T in favor of n and p. In its turn, p can be eliminated by integrating Eq. (1) over the whole box and using the Gauss theorem and Eq. (4). It is convenient to write the governing equations in a scaled form. Introduce scaled coordinates $\mathbf{r}/L_x\to\mathbf{r}$ so that the scaled box dimensions become $1\times\Delta$, where $\Delta=L_y/L_x$ is the aspect ratio of the box. Introducing the (scaled) inverse granular density $z(x,y)=n_c/n(x,y)$, we obtain

$$\boldsymbol{\nabla}\cdot[F(z)\boldsymbol{\nabla}z]=\mathcal{L}Q(z). \tag{5}$$

The boundary conditions are

$$\boldsymbol{\nabla}_n z=\mathbf{0} \quad \text{at } x=0,\ y=0,\ \text{and } y=\Delta, \tag{6}$$

and

$$\left.\left(G(z)\frac{\partial z}{\partial x}\right)\right|_{x=1}=\mathcal{L}\frac{\int_0^1\int_0^\Delta Q\,dx\,dy}{\int_0^\Delta H[z(1,y)]\,dy}. \tag{7}$$

The normalization condition becomes

$$\Delta^{-1}\int_0^1\int_0^\Delta z^{-1}\,dx\,dy=f, \tag{8}$$

while the functions F, G, H, and Q are the following:

$$F(z)=\frac{(z^2+2z-1)[\alpha z(z-1)+\sqrt{32/3}(z-a)]^2}{(z-a)(z-1)^{1/2}z^{3/2}(z+1)^{5/2}}, \tag{9}$$

$$G(z)=\frac{(z^2+2z-1)[\alpha z(z-1)+\sqrt{32/3}(z-a)]^2}{z(z-a)(z-1)(z+1)^2}, \tag{10}$$

$$H(z)=\frac{F(z)}{G(z)}, \quad \text{and } Q(z)=\frac{(z-a)(z-1)^{1/2}}{(z+1)^{3/2}z^{1/2}}. \tag{11}$$

Finally, $\mathcal{L}=(32/3\gamma)(L_x/d)^2(1-r^2)$. The other two governing parameters are the grain area fraction $f=\langle n\rangle/n_c$ and Δ. For an infinite strip $\Delta=\infty$, and one is left with only two governing parameters, $\mathcal{L}$ and f. Notice that the steady-state *density* distributions are independent of A and ω (in contrast to problems with nonzero gravity, where the gravity acceleration, combined with the maximum wall acceleration $A\omega^2$, forms an additional governing parameter).

Equations (5)–(8) make a closed set. Their one-dimensional (1D) (y-independent) solution $Z=Z(x)$ is described by the equations

$$(FZ')'=\mathcal{L}Q, \quad Z'|_{x=0}=0, \quad \text{and } \int_0^1 Z^{-1}dx=f, \tag{12}$$

where the primes stand for the x derivatives. Equation (7) is now satisfied automatically. Equations (12) coincide with those obtained by Grossman *et al.* [6] for a *thermal* wall at $x=1$. Therefore, the density profiles of the 1D states coincide for the different types of driving. Equations (12) can be solved analytically in the high- and low-density limits [6].

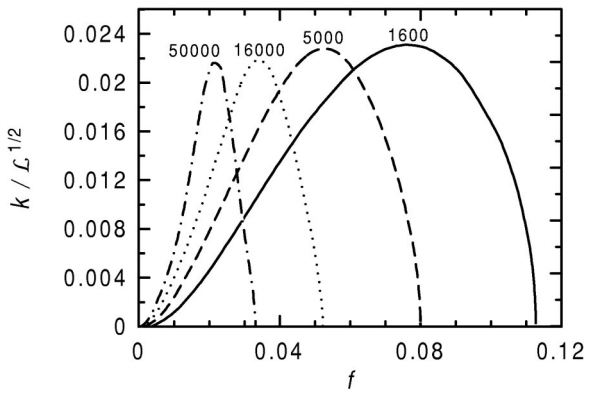

FIG. 1. Marginal stability curves $k_*(f)$ for different values of $\mathcal{L}$. The values of k_* are divided by $\mathcal{L}^{1/2}$. For a fixed $\mathcal{L}$ the ECS is unstable below the corresponding marginal stability curve.

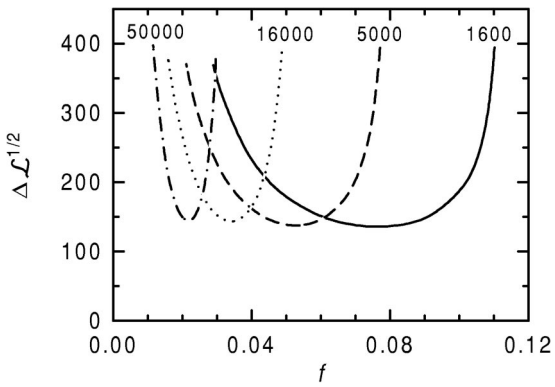

FIG. 2. Critical values of the aspect ratio $\Delta_1(f)$, needed for the instability to develop, for different values of $\mathcal{L}$. The values of Δ_1 are multiplied by $\mathcal{L}^{1/2}$.

These solutions clearly show that the criterion [10] for the validity of hydrodynamics is equivalent to a strong inequality $1-r^2 \ll 1$.

Most interesting among the 1D states is the state with a dense cluster (an ECS) located at the elastic wall $x=0$, and a low-density region elsewhere. In this case Eqs. (12) should be solved numerically. Examples are presented in Ref. [6], and a similar clustering state (CS) has been observed experimentally [9]. The main objective of this work is to show that this laterally uniform state can give way, via a spontaneous symmetry breaking, to CSs periodic in the lateral (y) direction. First, a marginal stability analysis will show loss of stability of the ECS in a certain region of parameters. Then, solving Eqs. (5)–(8) numerically, we will find that, well within the instability region, the density of the periodic CSs becomes strongly peaked in the lateral direction. Finally, time-dependent granular hydrodynamic simulations will show that strongly peaked CSs are dynamically stable and can develop from small-amplitude single-mode density perturbations in boxes of a finite size.

III. SYMMETRY-BREAKING INSTABILITY AND STRONGLY PEAKED PERIODIC STATES

We start with a marginal stability analysis of the ECS. Linearizing Eqs. (5)–(8) around the ECS $z=Z(x)$ and looking for a small correction in the form of $\psi_k(x)\cos(ky)$, where k is the lateral wave number, we obtain

$$F\phi'' - (\mathcal{L}Q_Z + k^2 F)\phi = 0. \tag{13}$$

Here $\phi = F\psi_k$ and the index Z means the z derivative evaluated at $z=Z(x)$. The boundary conditions are

$$\phi'|_{x=0} = 0, \quad [FG\phi' + Z'(FG_Z - GF_Z)\phi]|_{x=1} = 0. \tag{14}$$

The functions F and G that enter Eqs. (13) and (14) are evaluated at $z=Z(x)$.

For fixed values of $\mathcal{L}$ and f, Eqs. (13) and (14) represent a linear eigenvalue problem for the lateral wave number k. Let us first consider an infinite strip $\Delta \to \infty$, when these eigenvalues $k=k_*$ are continuous. Figure 1 shows, for different values of $\mathcal{L}$, the marginal stability curves $k_* = k_*(f)$ found numerically. For a fixed $\mathcal{L}$ the ECS is unstable for any $k < k_*(f)$, that is, below the corresponding marginal stability curve. Interestingly, the $k_*(f)$ curves have compact support: the ECS remains linearly stable for *any* k beyond a finite interval of the area functions $f_1(\mathcal{L}) < f < f_2(\mathcal{L})$ such that $f_1 > 0$ and $f_2 < 1$. As $\mathcal{L}$ increases, the instability interval (f_1, f_2) shrinks, while the maximum value of $k_*(f)$ increases. This increase can be approximately described as $k_*^{\max} \simeq (\pi/140)\mathcal{L}^{1/2}$. We used this approximate scaling in Fig. 1 to show, on a single graph, the marginal stability curves in a broad range of $\mathcal{L}$.

When $f \ll \min(1, \mathcal{L}^{-1/2})$, the asymptotics of $k_*(f)$ can be found analytically. In this case the whole granulate is in the dilute limit, $z \gg 1$ (still, it is necessary to account for the subleading terms). In addition, $Z(1) - Z(0) \ll Z(0)$ in this case, so Taylor expansion of $Z(x)$ and $\psi(x)$ up to x^4 suffices. After some algebra, Eqs. (12)–(14) yield

$$K_* = \left[\frac{\mathcal{L}^2 f^4}{3\alpha^4} - \frac{(1+a)\mathcal{L} f^3}{\alpha^2} \right]^{1/2}. \tag{15}$$

It follows from Eq. (15) that $f_1(\mathcal{L}) = 3\alpha^2(1+a)\mathcal{L}^{-1}$. Our numerical results shown in Fig. 1 are in excellent agreement with these predictions.

Therefore, marginal stability analysis predicts a symmetry-breaking instability of the ECS. For the infinite strip, the instability occurs on a finite interval of the wave numbers. In a system with finite lateral dimension the lateral wave number k is discrete because of the boundary conditions: $k = \pi m/\Delta$, where $m = 1,2,\ldots$. Let us fix $\mathcal{L}$ and f and find the critical values of the aspect ratio Δ_m, such that at $\Delta > \Delta_m$ the ECS loses stability with respect to the mth mode. Obviously, $\Delta_m(\mathcal{L}, f) = m\Delta_1(\mathcal{L}, f)$. For the mode $m=1$ (this mode can also be called $\lambda/2$, that is, one-half of the wavelength across the system in the lateral direction) the critical aspect ratio Δ_1 is the lowest. Figure 2 shows, for different values of $\mathcal{L}$, the critical aspect ratios $\Delta = \Delta_1(f)$. The symmetry-breaking instability develops in the parameter region *above* these curves (within instability tongues). Note

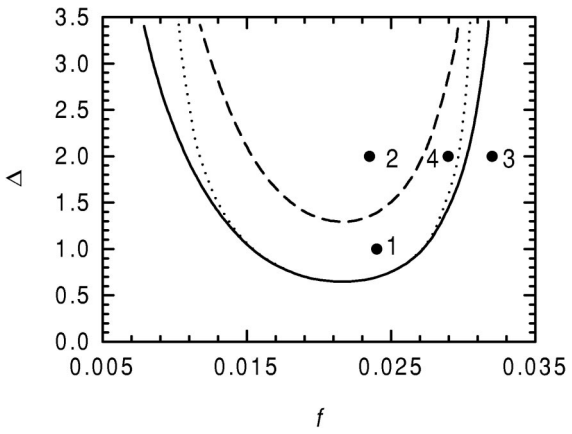

FIG. 3. Critical values of the aspect ratios $\Delta_m(f)$ for $m=1$ (solid line) and 2 (dashed line) and $\mathcal{L}=5\times10^4$. Two-dimensional density profiles corresponding to points 1, 2, 3, and 4 are shown below in Fig. 4. The dotted line shows the critical value $\Delta_1(f)$ for the ''thermal wall.''

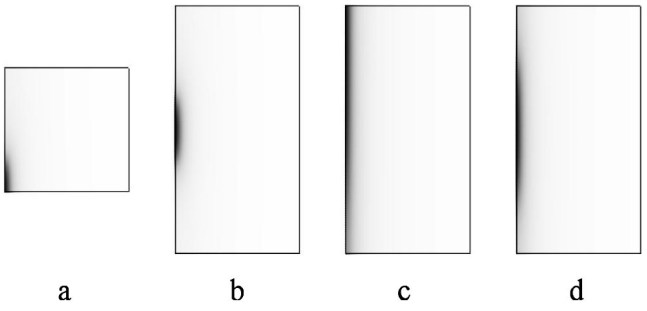

FIG. 4. Steady-state density profiles (gray scale, separate for each picture) corresponding to points 1(a), 2(b), 3(c), and 4(d) of Fig. 3. The maximum (minimum) density at the wall $x=0$ is 0.76 (0.036) (a) and (b), 0.48 (0.21) (c), and 0.54 (0.10) (d). The gas density at the vibrating wall $x=1$ is close to 4×10^{-3} for all profiles.

that these curves can be obtained from the curves shown in Fig. 1 by simply calculating $\Delta_1(f)=\pi/k_*(f)$ for the given $\mathcal{L}$.

For sufficiently large $\mathcal{L}$, $\Delta_1^{(\min)}$ becomes less than 1, so one does not need a long strip to observe the symmetry-breaking instability. Figure 3 shows the instability tongues $m=1$ and $m=2$ for $\mathcal{L}=5\times10^4$. For higher m we obtain modes 3λ/2, 2λ, 5λ/2,..., which fit in boxes with increasingly larger aspect ratios, $\Delta>m\Delta_1$.

We also found a similar symmetry-breaking instability when the wall $x=1$ (in scaled units) is ''thermal.'' Solving the corresponding eigenvalue problem [where the second boundary condition in Eq. (14) is replaced by $\phi(x=1)=0$], we obtained marginal stability curves similar to those for the vibrating wall, but more narrow. As an example, the dotted line in Fig. 3 shows the instability tongue $m=1$ in the case of a ''thermal'' wall for $\mathcal{L}=5\times10^4$. Noticeable is the coincidence of the $m=1$ curves at intermediate f for the two types of driving. This coincidence results from a strong localization of the eigenfunction $\phi(x)$ near the elastic wall $x=0$ at large $\mathcal{L}$ and intermediate f. The exact form of the boundary condition at $x=1$ becomes irrelevant in this regime. Finally, for the thermal wall the ECS is stable for any Δ if $f\ll\min(1,\mathcal{L}^{-1/2})$, in contrast to the vibrating wall.

In the rest of the paper we will deal with the vibrating wall. Within the instability region the marginal stability analysis is no longer valid. In addition, any linear analysis can miss a subcritical bifurcation outside the instability region. Therefore, we directly solved the two-dimensional steady-state equations (5)–(8) numerically (using a nonlinear Poisson solver and Newton's iterations), exploring some parts of the parameter plane (f,Δ) of Fig. 3. We worked with systems of finite lateral dimensions. The results of these calculations, however, are generalizable to an infinite strip. Indeed, the nonlinear Poisson equation (5) has a rich family of solutions periodic in y. Therefore, a numerical solution obtained for $0<y<\Delta$, and satisfying the no-flux boundary conditions at $y=0$ and $y=\Delta$, represents a natural ''building block'' of the corresponding nonlinear periodic solution (see below). Note that the weakly modulated (cosine-like) solutions, considered in our marginal stability analysis, represent a small-amplitude limit of these nonlinear periodic solutions.

Figure 4 shows two-dimensional density profiles of four typical steady states with $m=1$ and 2. Strongly peaked (highly nonlinear) λ/2 and λ states are evident in Figs. 4(a) and 4(b). Figure 5 shows the density profile along the elastic wall $x=0$, corresponding to Fig. 4(b). Strong localization of the granulate in the lateral direction is clearly seen. The maximum/minimum density ratio along the elastic wall is about 21 in this example.

A mirror reflection of Fig. 4(a) with respect to $y=0$ makes $\Delta=2$ and produces a λ state similar to that shown in Fig. 4(b). A nonlinear periodic solution for an infinite strip is obtained simply by extending Fig. 4(b) periodically in the y direction. This strongly peaked periodic solution looks like an infinite chain of ''islands,'' or strongly localized CSs. Obviously, cluster chains with different periods can fit in the infinite strip (actually, even in finite boxes with large enough aspect ratios). Therefore, an interesting nonlinear selection problem arises, as in other pattern-forming systems [11]. One can expect that pattern selection will occur via competition between clusters for material and their coarsening.

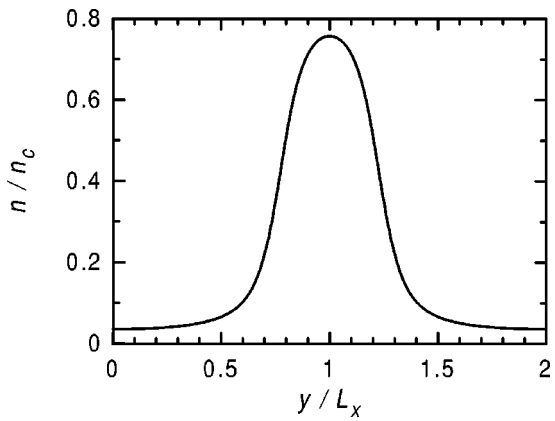

FIG. 5. Density profile along the elastic wall $x=0$, corresponding to Fig. 4(b).

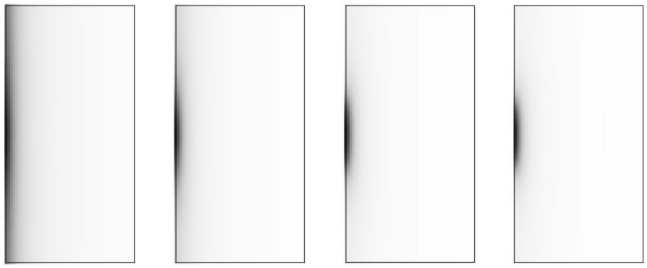

FIG. 6. Density evolution for $\mathcal{L}=5\times10^4$, $\Delta=2$, and $f=0.0235$. Shown are the density profiles (gray scale, separate for each picture) at scaled times 100 (a), 500 (b), 1000 (c), and 1290 (d). The maximum (minimum) density at the wall $x=0$ is 0.25 (0.14) (a), 0.46 (0.072) (b), 0.66 (0.040) (c), and 0.74 (0.036) (d). The gas density at the vibrating wall $x=1$ is close to 4×10^{-3} for all profiles.

In general, we found that, when crossing the curve $\Delta=\Delta_1(f)$ (see Fig. 3) from the left (along the line $\Delta=2$), or from below, one goes continuously from an ECS to a ''weakly two-dimensional'' $\lambda/2$ state. This implies a supercritical bifurcation. However, when moving from the right to the left along the line $\Delta=2$, nonlinear $\lambda/2$ and λ states appear inside the linear stability regions of the ECS and of the mode $m=1$, respectively, and coexist with the ECS and with the mode $m=1$, respectively. These findings give evidence for bistability and subcritical bifurcations. Examples of subcritical $\lambda/2$- and λ states are shown in Figs. 4(c) and 4(d). We also observed super- and subcritical strongly peaked periodic CSs for $\Delta=3$.

Are the localized CSs dynamically stable, and can they develop from small-amplitude initial perturbations around a uniform state? We performed a series of time-dependent hydrodynamic simulations with $\Delta=1$, 2, and 3 that gave positive answers to these questions. We will briefly report here a single simulation with $\Delta=2$. The full hydrodynamic equations were solved with the same constitutive relations and boundary conditions as in the steady-state analysis. Instead of the shear viscosity in the momentum equation we accounted for a small model friction force $-n\mathbf{v}/\tau$. An extended version of the compressible hydro code VULCAN [15] was used.

The initial scaled density in this example included a single-mode perturbation $n(x,y,t=0)=f+0.1f\cos(\pi y)$ (independent of x). Figure 6 shows the density evolution. A cluster develops near the elastic wall $x=0$. With time it becomes strongly peaked in the y direction and approaches the steady-state profile shown in Fig. 4(c).

IV. DISCUSSION AND CONCLUSIONS

We predict a spontaneous transition from a laterally uniform clustering state to highly peaked periodic clustering states in a driven submonolayer granular system. The transition should occur when the aspect ratio of the system is large enough, and the area fraction of the granulate belongs to the interval (f_1,f_2). The transition is insensitive to the vibration frequency and amplitude, and depends only weakly on the type of driving wall (under the conditions delineated above). An important selection issue (what is the wavelength of the resulting pattern in an infinite, or long enough, strip?) is yet unresolved. We expect that selection will occur via competition between clusters for material, and their coarsening. Overall, our results put this simple system in the list of pattern-forming systems out of equilibrium [11].

The symmetry-breaking instability predicted in this work does not require very special constitutive relations. We checked that it appears already in the dilute limit, $n\ll n_c$, where the constitutive relations are directly derivable (in the nearly elastic limit) from the Chapman-Enskog expansion of the kinetic theory [16]. Very recent calculations [17] show that the main features of the instability remain the same if one uses, instead of the constitutive relations of Ref. [6], the ''standard'' relations obtained by Jenkins and Richman [5]. There are some quantitative differences, however, in the precise locations of the marginal stability curves [17]. Therefore, the symmetry-breaking instability provides a sensitive test for the accuracy of different constitutive relations. Recently, a new ''global equation of state'' in 2D was proposed [18] that uses a more refined interpolation than in Ref. [6] between the dilute, intermediate, and dense limits, and agrees very well with particle simulations. We expect that when a similar interpolation for the ''global heat conductivity'' becomes available, the marginal stability curves will be computed with a higher precision.

It should be straightforward to observe the symmetry-breaking instability in particle simulations. We hope it will also be observed in experiment. Note that the aspect ratios used in the previous particle simulations [6,7] and experiment [9] were always lower than the critical values for the instability, $\Delta_1^{(\min)}$. As a result, the instability was suppressed by granular heat conduction in the lateral direction. In planning the experiment, one should try to minimize the role of the rolling/sliding friction [9], unaccounted for in our model. The frictional energy losses are proportional to $T^{1/2}$, while the collisional energy losses are proportional to $T^{3/2}$. Therefore, one should work with high granular temperatures (that is, large $A\omega$).

When $1-r^2$ is not small, the normal stress difference, non-Gaussianity in the velocity distribution, and possible lack of scale separation all become important. The role of these effects in the symmetry-breaking instability should be the subject of further studies.

ACKNOWLEDGMENTS

We acknowledge useful discussions with E. Ben-Naim, J. Fineberg, J. P. Gollub, L. P. Kadanoff, S. Luding, and S. W. Morris. This research was supported by the Israel Science Foundation founded by the Israel Academy of Sciences and Humanities, and by the Russian Foundation for Basic Research (Grant No. 99-01-00123).

[1] H. M. Jaeger, S. R. Nagel, and R. P. Behringer, Rev. Mod. Phys. **68**, 1259 (1996); Phys. Today **49**(4), 32 (1996).
[2] L. P. Kadanoff, Rev. Mod. Phys. **71**, 435 (1999).
[3] M. A. Hopkins and M. Y. Louge, Phys. Fluids A **3**, 47 (1991); I. Goldhirsch and G. Zanetti, Phys. Rev. Lett. **70**, 1619 (1993); S. McNamara and W. R. Young, Phys. Rev. E **53**, 5089 (1996).
[4] Similar thermal condensation instabilities develop in radiatively cooling plasmas; for a review, see B. Meerson, Rev. Mod. Phys. **68**, 215 (1996).
[5] J. T. Jenkins and M. W. Richman, Phys. Fluids **28**, 3485 (1985); C. S. Campbell, Annu. Rev. Fluid Mech. **22**, 57 (1990).
[6] E. L. Grossman, T. Zhou, and E. Ben-Naim, Phys. Rev. E **55**, 4200 (1997).
[7] J. J. Brey and D. Cubero, Phys. Rev. E **57**, 2019 (1998).
[8] S. E. Esipov and T. Pöschel, J. Stat. Phys. **86**, 1385 (1997).
[9] A. Kudrolli, M. Wolpert, and J. P. Gollub, Phys. Rev. Lett. **78**, 1383 (1997).
[10] Hydrodynamics is expected to be valid when the mean free path of the grains is much smaller than any length scale (and the mean collision time is much smaller than any time scale) described hydrodynamically.
[11] M. C. Cross and P. C. Hohenberg, Rev. Mod. Phys. **65**, 851 (1993).
[12] Ref. [7] actually used constant (and equal) temperatures at two opposite walls.
[13] S. McNamara and S. Luding, Phys. Rev. E **58**, 813 (1998), and references therein.
[14] V. Kumaran, Phys. Rev. E **57**, 5660 (1998).
[15] E. Livne, Astrophys. J. **412**, 634 (1993).
[16] J. J. Brey and D. Cubero, in *Granular Gases*, edited by T. Pöschel and S. Luding (Springer, Berlin, 2001), pp. 59–78; I. Goldhirsch, *ibid.*, pp. 79–99.
[17] Y. Khain and B. Meerson (unpublished).
[18] S. Luding and O. Strauss, in *Granular Gases* (Ref. [16]), pp. 389–409; S. Luding, Phys. Rev. E **63**, 042201 (2001).